Defense Technical Information Center Compilation Part Notice

ADP010724

TITLE: Large-Amplitude, High-Rate Roll Oscillation sof a 65 Deg. Delta Wing at High Incidence

DISTRIBUTION: Approved for public release, distribution unlimited

This paper is part of the following report:

TITLE: Verification and Validation Data for Computational Unsteady Aerodynamics [Donnees de verification et de valadation pour l'aerodynamique instationnaire numerique]

To order the complete compilation report, use: ADA390566

The component part is provided here to allow users access to individually authored sections of proceedings, annals, symposia, ect. However, the component should be considered within the context of the overall compilation report and not as a stand-alone technical report.

The following component part numbers comprise the compilation report:

ADP010704 thru ADP010735

16C. LARGE-AMPLITUDE, HIGH-RATE ROLL OSCILLATIONS OF A 65^O DELTA WING AT HIGH INCIDENCE

Neal M. Chaderjian and Lewis B. Schiff
NASA Ames Research Center
Moffett Field, California, U.S.A.

INTRODUCTION

The IAR/WL 65° delta wing experimental results provide both detail pressure measurements and a wide range of flow conditions covering from simple attached flow, through fully developed vortex and vortex burst flow, up to fully-stalled flow at very high incidence. Thus, the Computational Unsteady Aerodynamics researchers can use it at different level of validating the corresponding code. In this section a range of CFD results are provided for the 65° delta wing at selected flow conditions. The time-dependent, three-dimensional, Reynolds-averaged, Navier-Stokes (RANS) equations are used to numerically simulate the unsteady vortical flow. Two sting angles and two large-amplitude, high-rate, forced-roll motions and a damped free-to-roll motion are presented. The free-to-roll motion is computed by coupling the time-dependent RANS equations to the flight dynamic equation of motion. The computed results are compared with experimental pressures, forces, moments and roll angle time history. In addition, surface and off-surface flow particle streaks are also presented.

LIST OF SYMBOLS AND DEFINITIONS

B	wing span, (in)
c	root chord, (in)
c_0	mean aerodynamic chord, (in)
C_p	pressure coefficient $=(p-p_0)/qs$
C_ℓ	rolling moment coefficient $=\ell/qsB$
C_N	normal force coefficient =N/qs
f	frequency, (Hz)
k	reduced frequency $=\pi fB/V_0$
ℓ	rolling moment, (lbs-in)
M_∞	Mach number
m	pitching moment, (lbs-in)
N	normal force, (lbs)
n	yawing moment, (lbs-in)
p	pressure, (psi)
p_0	static pressure, (psi)
q	dynamic pressure, (psi)
Re	Reynolds number, based on root chord
s	wing area, (in^2)
S	semi span, (in)
T_0	static temperature, (°C)
t	time (sec)
V_0	free stream velocity (ft/sec)
x,y,z	body axes coordinates
X_{Cp}	center of pressure in x axis, (in)
α	angle of attack, (°)
σ	sting angle (between body axis and tunnel axis), (°)
ϕ	roll angle, (°)
ϕ_0	mean roll angle or initial roll angle, (°)
$\Delta\phi$	amplitude, (°)

$\dot{\phi}$	roll angular rate, (rad/sec)
CCW	counter clockwise
CW	clockwise
CFD	Computational Fluid Dynamics
NSS	Navier-Stokes Simulation
RANS	Reynolds-averaged, Navier-Stokes Equations

FORMULARY

General Description of model

1.1	Designation	IAR Delta Wing
1.2	Derivation	IAR Dynamic Experimental Model
1.3	Type	Full model
1.4	References	Ref. 1 (Fig. 1)

Model Geometry

2.1	Planform	Delta wing-body, See Fig. 1
2.2	Aspect ratio	1.866
2.3	Mean aerodynamic chord	16.323 in
2.4	Root chord	24.485 in
2.5	Span	22.835 in
2.6	Reference center	13.875 aft of the apex
2.7	Leading edge sweep	65°
2.8	Trailing edge sweep	0°
2.9	Taper ratio	0
2.10	Twist	0°
2.11	Dihedral	0°
2.12	Area of planform	279.486 in^2
2.13	Leading-edge bevel (leeward)	9° (perpendicular to leading-edge)
2.14	Leading-edge bevel (windward)	9° (perpendicular to leading-edge)
2.15	Trailing edge bevel (leeward)	9° (perpendicular to trailing edge)
2.16	Trailing edge bevel (windward)	9° (perpendicular to trailing edge)
2.17	Leading-edge radius	0.020 in
2.18	Tolerance of leading-edge radius	±10%
2.19	Definition of profiles	0.375 inch thick flat-plate wing with double-bevelled (18° included angle) sharp leading and trailing edge
2.20	Center body	Ogive-cylinder
2.21	Form of wing-body junction	Bevelled, see Fig. 1
2.22	Form of wing tip	Sharp
2.23	Control surface details	None
2.24	Center-body diameter	3.150 in
2.25	Radius of forebody	$r = \sqrt{24.103^2 - (12.243 - x)^2} - 22.528$ in
2.26	References	Ref. 1 (Fig. 1)

CFD Grid Details

3.1	RANS grid size	67 axial x 209 circumferential x 49 normal points (baseline grid); 113 x 421 x 97 points (finest grid), See Fig. 2
3.2	Additional Remarks	Full-body grids used in all cases; zonal grids used in axial directio to fit machine memory; zonal boundaries are one-to-one matching

CFD Code used

4.1	RANS code	Novier-Stokes Simulation (NSS) code, Beam-Warming, block or diagonal, central differencing, blended 2nd- and 4th-order dissipation, reduced dissipation in boundary layer
4.2	Turbulence model	Baldwin-Lomax with Degani-Schiff modifications, no fixed transition
4.3	Computational time step	$3.62 \times 10^{-3} < \tau < 5.0 \times 10^{-3}$, 6.67×10^{-6} sec $< \Delta t < 9.0 \times 10^{-6}$ sec
4.4	Computation time	80 hours per oscillation cycle on a CRAY C-90 single processor - block version (15,000 steps per cycle of oscillation)
4.5	Additional remarks	Unsteady computation started with steady solution at ϕmax. Solution converged after 2-3 cycles
4.6	Reference on code	Ref. [5]

Model Motion

5.1	Mode of applied motion	Sinusoidal roll oscillations and free-to-roll motion about longitudinal axis of symmetry
5.2	Range of amplitude	28.2°, 31.9°, 40.0°
5.3	Reduced frequency	f = 7 Hz, 10 Hz; k = 0.14, 0.20
5.4	Additional Remarks	oscillations about ϕ_0 = 0.0°, 28.0°

Boundary Conditions

6.1	Mach Number	0.27
6.2	Reynolds Number	$Re_c = 3.67 \times 10^6$, based on root chord
6.3	Temperature	300° K
6.4	Range of model incidence	15° and 30°
6.5	Definition of model incidence	Model incidence defined relative to model axis of symmetry
6.6	Additional Remarks	Distance of far field boundary is 5 root chords normal to wing, 2 root chords upstream and downstream of wing

Data Presentation

7.1	Static Cases	Roll moment versus roll angle
		Normal force versus roll angle
		Center of pressure versus roll angle
		Leeward surface pressure distributions for various roll angles
		Surface flow patterns for various roll angles
		Vortex breakdown point versus roll angle
7.2	Forced Roll Oscillations	Instantaneous roll moment versus roll angle
		Instantaneous normal force versus roll angle
		Center of pressure versus roll angle
7.3	Free-to-Roll Oscillations	Roll angle history versus time
7.4	Sample illustrations	Fig. 3 to Fig. 10

7.5	Additional Remarks	All above quantities are compared against IAR experiments (Case No. 2, No. 3, No. 5, No. 6 and No. 10)

Personal contact for further information

Dr. Neal M. Chaderjian, T27B-2, NASA Ames Research Center, Moffett Field, California U. S. A
Phone: (650) 604-4472, E-mail: nchaderjian@mail.arc.nasa.gov

List of references

[1]. N. M. Chaderjian, "Navier-Stokes Prediction of Large-Amplitude Delta-Wing Roll Oscillations," *Journal of Aircraft*, Vol. 31, No. 6, pp. 1333-1340.

[2]. N. M. Chaderjian and L. B. Schiff, "Navier-Stokes Prediction of a Delta Wing in Roll with Vortex Breakdown," AIAA Paper 93-3495, 11th Applied Aerodynamics Conference, Monterey CA, August 1993.

[3]. N. M. Chaderjian and L. B. Schiff, "Numerical Simulation of Forced and Free-to-Roll Delta-Wing Motions," *Journal of Aircraft*, Vol. 33, No. 1, pp. 93-99.

[4]. N. M. Chaderjian and L. B. Schiff, "Navier-Stokes Analysis of a Delta Wing in Static and Dynamic Roll," AIAA Paper 95-1868, 13th Applied Aerodynamics Conference, San Diego, CA, June 1995.

[5]. N. M. Chaderjian, "Comparison of Two Navier-Stokes Codes for Simulating High-Incidence Vortical Flow", *Journal of Aircraft*, Vol. 30, No. 3, pp. 357-364.

[6]. E. S. Hanff and X. Z. Huang, "Roll-Induced Cross-Loads on a Delta Wing at High Incidence," AIAA Paper 91-3223, September 1991

[7]. E. S. Hanff and S.B. Jenkins, "Large-Amplitude High-Rate Roll Experiments on a Delta and Double Delta Wing," AIAA paper 90-0224, January 1990.

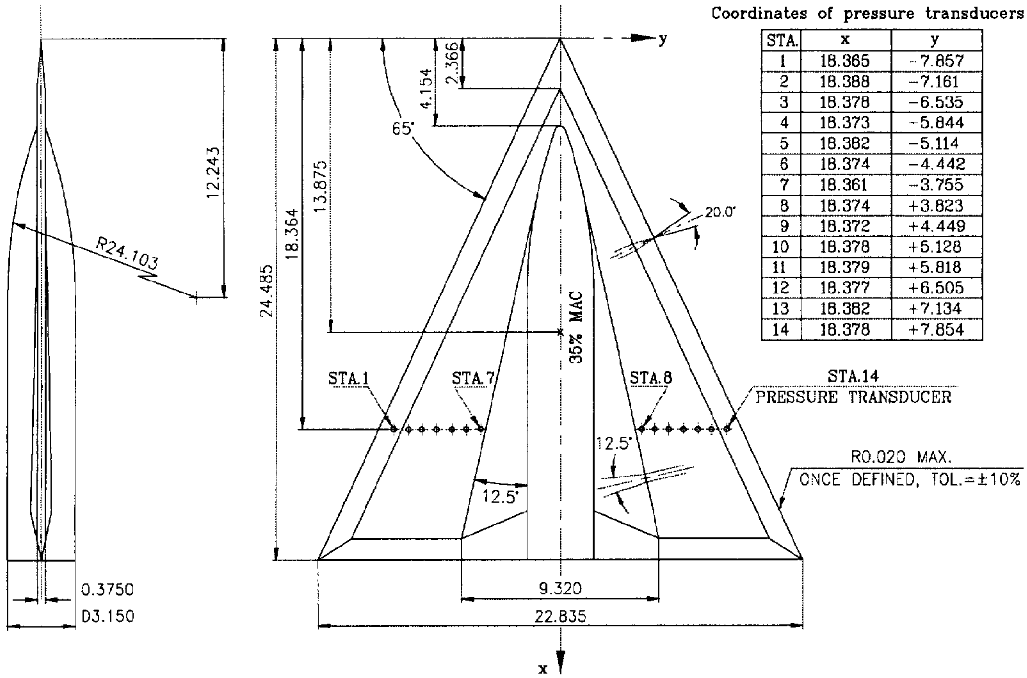

STA.	x	y
1	18.365	-7.857
2	18.388	-7.161
3	18.378	-6.535
4	18.373	-5.844
5	18.382	-5.114
6	18.374	-4.442
7	18.361	-3.755
8	18.374	+3.823
9	18.372	+4.449
10	18.378	+5.128
11	18.379	+5.818
12	18.377	+6.505
13	18.382	+7.134
14	18.378	+7.854

Fig. 1 65° delta wing model

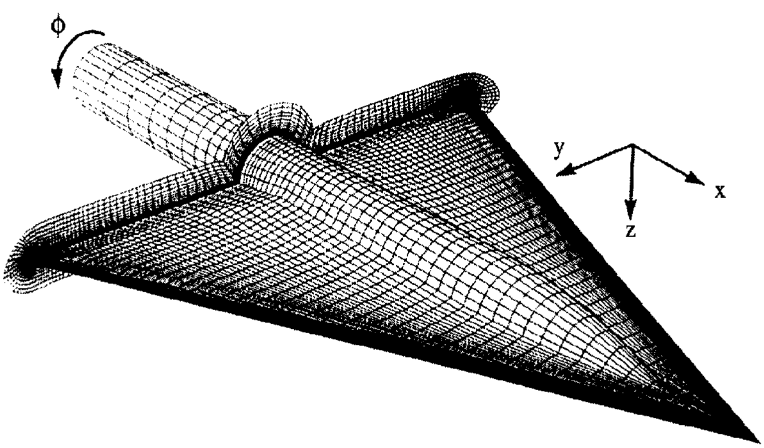

Fig. 2 Perspective view of the computational grid

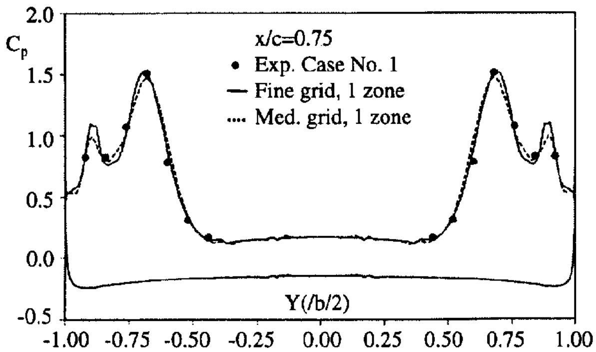

Fig. 3 Effects of grid refinement and zonal boundary condition treatment on the pressure coefficients
M_∞=0.27, α=15°, ϕ=0, Re=3.67 million

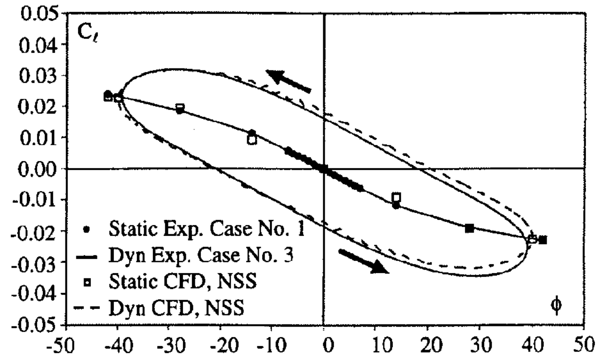

Fig. 4 Comparison of computational and experimental rolling moment coefficients for dynamic and static cases
M_∞=0.27, σ=15°, $\Delta\phi$=40°, k=0.14, Re=3.67 million

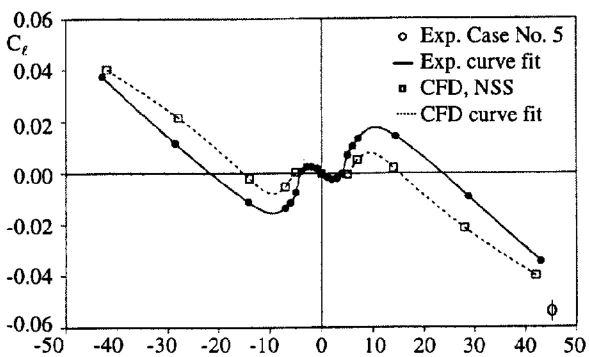

Fig. 5 Comparison of mean computed and experimental rolling moment coefficients for static roll angles
M_∞=0.27, σ=30°, Re=3.67 million

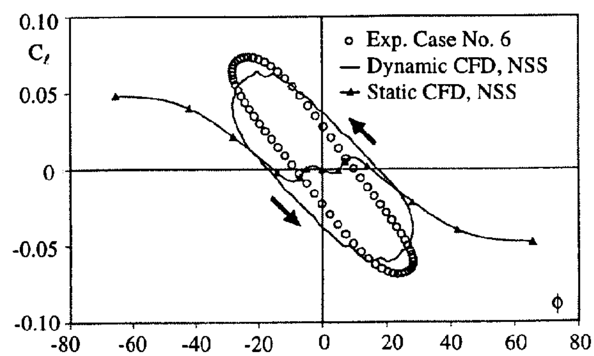

Fig. 6 Dynamic and static rolling-moment coefficients
M_∞=0.27, σ=30°, ϕ_0=0°, $\Delta\phi$=28.2°, k=0.20, Re=3.67 million

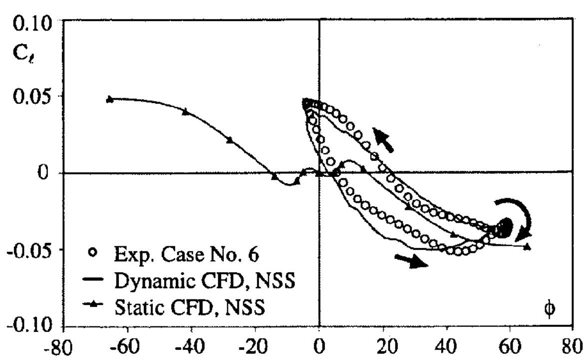

Fig. 7 Dynamic and static rolling-moment coefficients
M_∞=0.27, σ=30°, ϕ_0=28°, $\Delta\phi$=31.9°, Re=3.67 million

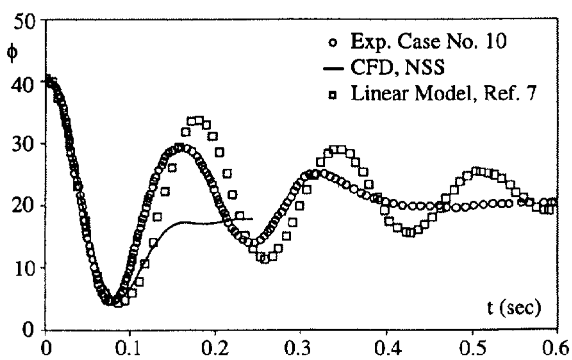

Fig. 8 Time history of roll angle for free-to-roll motion
M_∞=0.27, σ=30°, ϕ_0=40.5°, Re=3.67 million

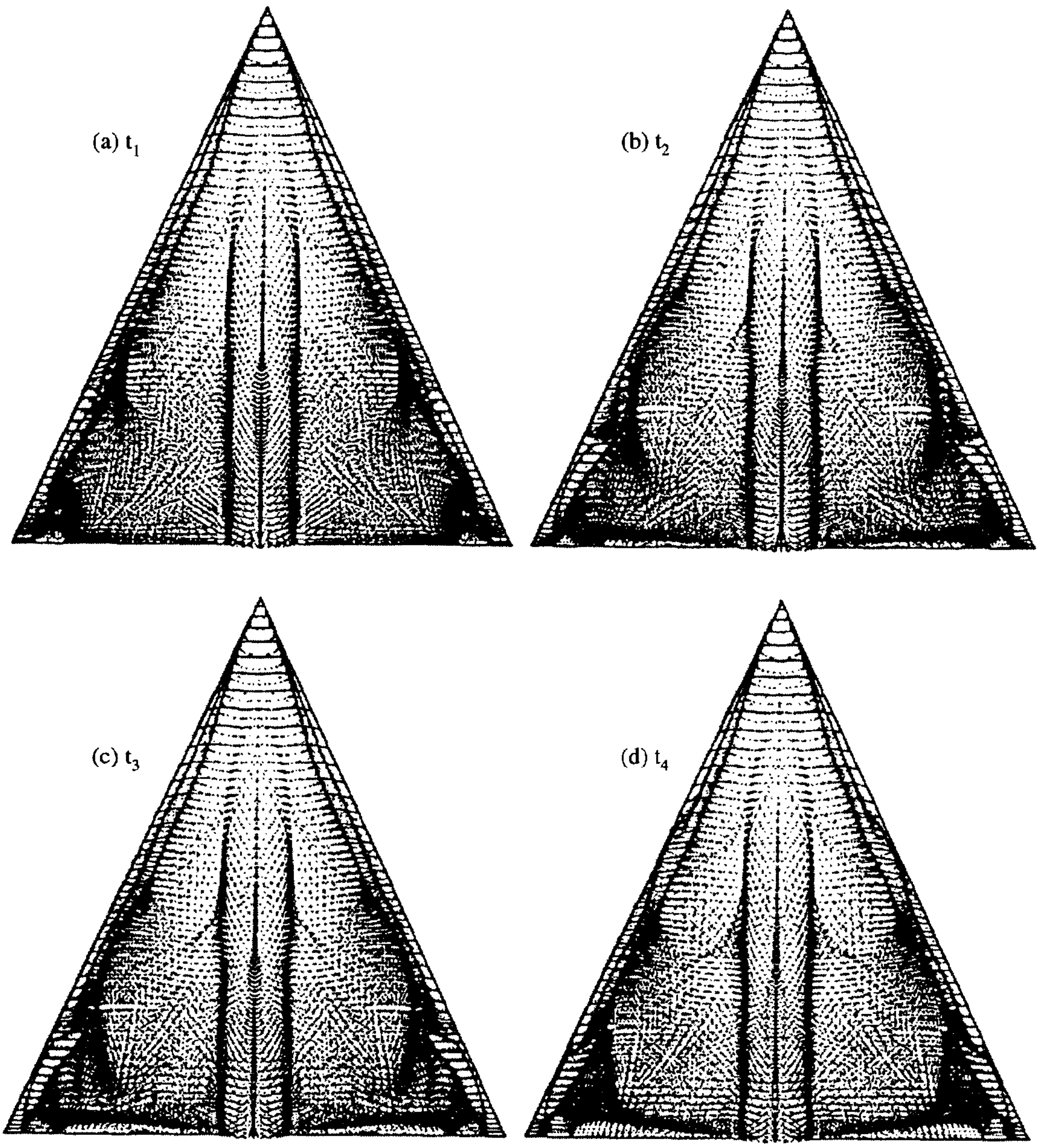

Fig. 9 Computed unsteady surface-flow particle-streaks at four sequential times
M_∞=0.27, α=30°, φ=0°, Re=3.67 million

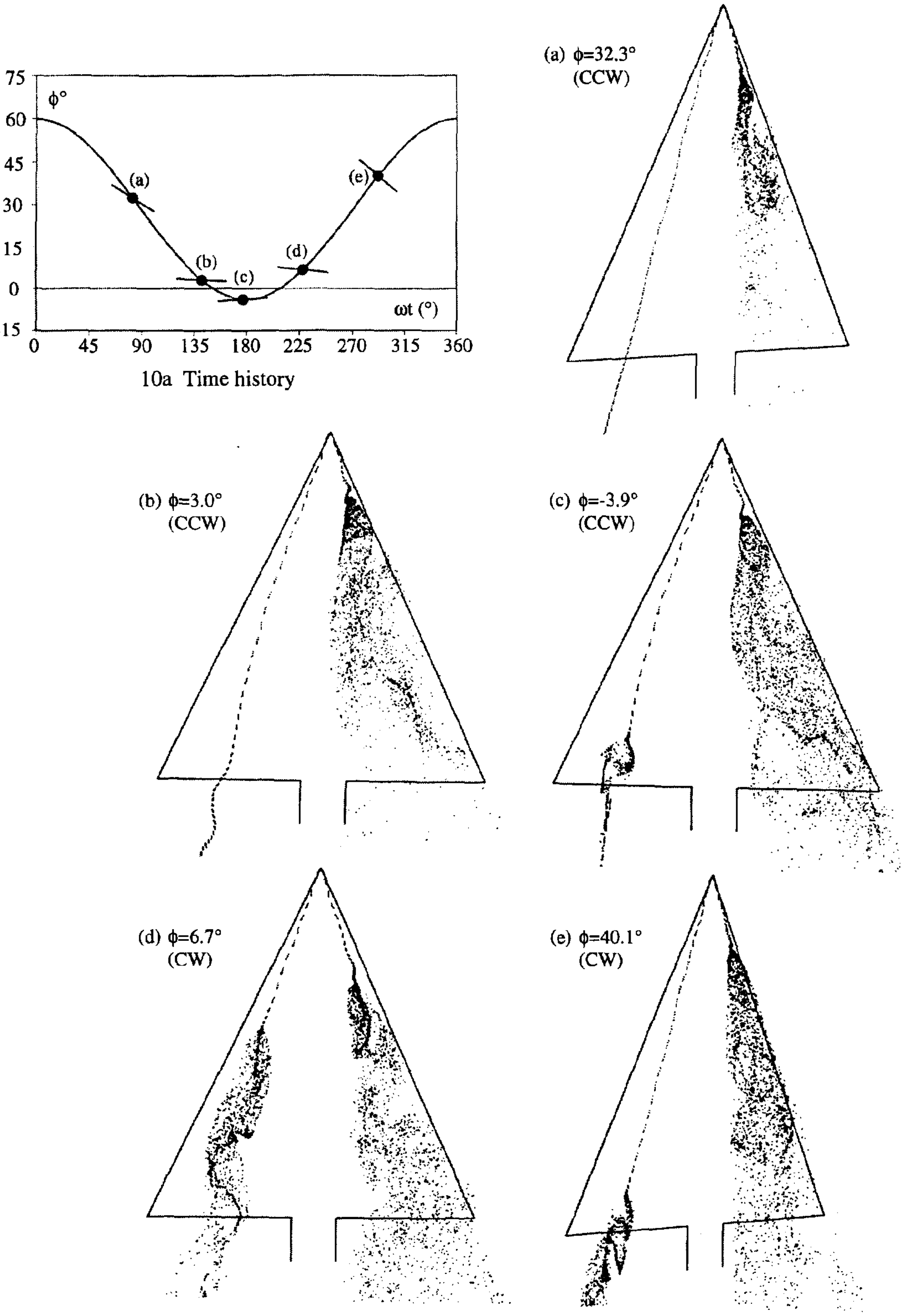

Fig. 10 Periodic formation and disappearance of vortex breakdown over left wing
M_∞=0.27, α=30°, ϕ_0=28°, $\Delta\phi$=31.9°, k=0.20, Re=3.67 million